Millisecond timescale slimfield imaging and automated quantification of single fluorescent protein molecules for use in probing complex biological processes

Michael Plank,†[a] George Howard Wadhams[b] and Mark Christian Leake*[ab]

Fluorescence microscopy offers a minimally perturbative approach to probe biology *in vivo*. However, available techniques are limited both in sensitivity and temporal resolution for commonly used fluorescent proteins. Here we present a new imaging system with a diagnostic toolkit that caters for the detection and quantification of fluorescent proteins for use in fast functional imaging at the single-molecule level. It utilizes customized microscopy with a mode of illumination we call "slimfield" suitable for rapid ($\sim$millisecond) temporal resolution on a range of common fluorescent proteins. Slimfield is cheap and simple, allowing excitation intensities $\sim$100 times greater than those of widefield imaging, permitting single-molecule detection at high speed. We demonstrate its application on several purified fluorescent proteins in standard use as genetically-encoded reporter molecules. Controlled *in vitro* experiments indicate single protein molecules over a field of view of $\sim$30 μm^2 area, large enough to encapsulate complete prokaryotic and small eukaryotic cells. Using a novel diagnostic toolkit we demonstrate automated detection and quantification of single molecules with maximum imaging rates for a 128 $\times$ 128 pixel array of $\sim$500 frames per second with a localization precision for these photophysically poor fluorophores to within 50 nm. We report for the first time the imaging of the dim enhanced cyan fluorescent protein (ECFP) and CyPet at the single-molecule level. Applying modifications, we performed simultaneous dual-colour slimfield imaging for use in co-localization and FRET. We present preliminary *in vivo* imaging on bacterial cells and demonstrate $\sim$millisecond timescale functional imaging at the single-molecule level with negligible photodamage.

Introduction

Use of fluorescent proteins

The use of genetically-encoded fluorescent proteins (FPs) as reporter dye molecules for *in vivo* fluorescence imaging is a

powerful, well characterized experimental approach for investigating biological processes in intact cells. The marine jellyfish, *Aequorea victoria*, produces the naturally fluorescent molecule green fluorescent protein (GFP),[1] discovered in 1962 and now known to be utilized by many different ocean species which inhabit water depths where light struggles to penetrate. This natural form of GFP is excited maximally at a wavelength of $\sim$395 nm in the "far" ultraviolet, corresponding to a clear peak in the transmission curve of water.[2] A breakthrough in the application of GFP came with the cloning of its gene in 1992.[3] Subsequently, the gene has been expressed into several foreign hosts, including both prokaryotes and eukaryotes,[4,5] demonstrating that no biological catalysts specific to jellyfish are needed for this luminescence.

[a] *Clarendon Laboratory, Oxford Physics, Oxford University, Parks Road, Oxford, UK OX1 3PU. E-mail: m.leake1@physics.ox.ac.uk; Fax: +44 (0)1865 272400; Tel: +44 (0)1865 282559*
[b] *Oxford Centre for Integrative Systems Biology, Dept. of Biochemistry, Oxford University, South Parks Road, Oxford, UK OX1 3QU*
† Current address: University of Vienna, Dr-Karl-Lueger-Ring, 1010 Vienna, Austria.

Insight, innovation, integration

Many biological processes occur on a timescale of milliseconds. Investigations at the single-molecule level whilst retaining functionality is difficult to achieve with existing technology. Previously, functional imaging using fluorescent proteins was limited to events over a timescale of tens of milliseconds, and the observation of slow, membrane processes. Here we report an innovative imaging hardware and software package permitting detection and quantification of fluorescent proteins in single cells at $\sim$500 frames per second. We have integrated this technology towards addressing outstanding biological questions by demonstrating its use *in vitro* on several different fluorescent proteins at the single-molecule level and reporting preliminary data for its application to live-cell imaging. This non-invasive imaging package will provide unprecedented insight into fast *in vivo* processes.

Molecular biology advances allowed controlled mutation of the GFP gene, producing variants that are both brighter than the natural form, mature faster and are excited using visible light over a range of different colours.[6] The GFP-variant genes can then be fused to a gene encoding an unrelated protein in a foreign organism generating a single-molecule fluorescent tag for every one of the expressed protein molecules. Several GFP orthologs have been discovered, found in classes as diverse as corals, crustacea and sea anemones. Over the past decade the use of the GFP family as molecular reporters in living organisms has increased tremendously.[7,8] They have been utilized widely as non-invasive probes to study biological processes, from the level of the whole organism[9] to single cells[10] and to measure a cell's internal chemical environment.[11–13]

More recently, using advanced microscopy techniques the GFP tag can be excited into fluorescence and single molecules imaged in functional living cells with a sub-second time resolution.[14–17] However, to date, pushing true 2D imaging across an area of tens of square microns relevant to small cells to integration times below 10 ms per image frame whilst still retaining single-molecule precision has presented a significant technical challenge when looking at fluorescent proteins *in vivo*.

FPs in single-molecule microscopy

Single fluorescent molecules excited by a laser of appropriate intensity emit sufficient light to be visualized by a high-sensitivity video camera.[18] However, in the heterogeneous solvated environment of the living cell a major challenge of single-molecule microscopy, for which the signal-to-noise ratio is of the order of ~ 1, lies in the reduction of background noise (in the form of scattering, luminescence and cellular auto-fluorescence, in addition to detector readout, shot and "dark" noise) to produce an enhancement of the imaging contrast sufficient to permit detection of the underlying single-molecule signal. For example, Sase *et al.* previously reported the use of an optimized epifluorescence microscope to visualize single fluorophores on moving actin[19] using low background epifluorescence microscopy (LBEFM).[20] Another powerful high-contrast mode of fluorescence illumination often used for visualizing single FPs is total internal reflection microscopy (TIRF).[20–24] Here, the excitation light, typically from a laser source, is directed onto a glass microscope slide or coverslip from a steep angle of incidence above the so-called critical angle, resulting in the beam being reflected at the boundary of the microscope slide with the aqueous medium in which the biological sample is bathed. A caveat to this is that the reflection generates an evanescent field extending into the water solution. This decays exponentially with distance from the slide; the 1/e depth of penetration is wavelength-dependent but for typical visible light excitation this equates to ~ 100 nm. The relevance of this is that only fluorescent molecules very close to the interface are excited, whereas ones in the rest of the sample, or any fluorescent contamination present in the surrounding media, are not. This delimited excitation volume can thus increase the imaging contrast to such an extent that detection of single molecules in living samples within this thin ~ 100 nm slice becomes possible. In practice, for a living cell

this means it is an ideal method to monitor processes occurring in or very near to the cell membrane. However, it is not possible to apply this to deeper imaging, for example to monitor proteins in the cell cytoplasm. In addition, the laser excitation intensities available for this widefield technique are relatively low (typically in the range 10–100 W cm^{-2}). This imposes a limit on the maximum photon emission flux from a single fluorescent protein molecule which, as the imaging integration time is reduced to below ~ 100 ms per frame, typically results in the effective signal per frame having a comparable level to the camera noise, thereby preventing detection.

To image deep inside the interior of cells other illumination modes have been employed. For example, confocal fluorescence microscopy is a well-established technique for functional biological imaging,[25] which achieves high resolution, especially along the optical axis.[26] The principal drawback of this technique is that scanning of the sample is required for imaging, which leads to strict limitations as far as the temporal resolution is concerned, integration times being typically of the order of seconds. In addition, further resolution improvements in deep *in vivo* imaging can be made by employing multi-photon excitation, such as two-photon laser scanning microscopy. Here, excitation with two photons of half the transition-energy is required for the fluorescence process, and the fluorescent signal depends quadratically on the illumination intensity.[27–31] This technique has been successfully applied at the single-molecule level to organic dye molecules,[32] but produces inconsistent results when applied to living cells, partly due to autofluorescence saturation of the detected pixel intensity at the wavelengths used, which results from the presence of NADH and FAD.[33] In addition, the excitation intensity required is often considerable, resulting in measurable photodamage. The technique is also similar to confocal in suffering from a poor time resolution due to slow lateral scanning.

None of the existing fluorescence microscopy technologies can offer a fast imaging technique permitting millisecond-level imaging applicable to dynamic processes in the cell cytoplasm across the full extent of the cell and still have the sensitivity to detect single fluorescent protein molecules. Raster image correlation spectroscopy (RICS) is an exciting new technique which permits microsecond timescale collection of data from individual camera pixels, and typically millisecond timescale data from individual pixel line scans.[34] However, compiling a complete true 2D image across a field of view large enough to encapsulate even the smallest living cell takes typically $\sim$ seconds to acquire,[35] making this technique poor at the present time for observing fast $\sim$ millisecond events extended across a whole cell. Having a technique capable of performing this imaging over a millisecond timescale across an area of tens of square microns would be highly desirable as it would permit real-time molecular-level imaging of several biological processes which to date have only been explored under fixed or significantly slowed *in vitro* conditions. Here we present a new imaging hardware and software package which will now permit this. It consists of a focussed Gaussian-profile laser expanded laterally over the sample plane to permit "slimfield" imaging of small living cells. This relatively simple

optical trick has been used for several years in both confocal laser-scanning microscopy (CLSM) and in fluorescence correlation spectroscopy (FCS) to adjust the size of the confocal volume,[36] and in a modified format using a defocussing lens on a commercial fluorescence microscope was used previously to monitor single photophysically favourable organic dyes molecules *in vitro* at frame rates of ~ 200 Hz.[37] However, its application in fast *functional* 2D imaging using fully automated quantification of fluorescent proteins in live-cell samples has yet to be demonstrated. Here, we have now tested the approach using a variety of different commonly-employed fluorescent proteins both *in vitro* and *in vivo* and have shown that the high excitation intensity allows us to image at fast frame rates of ~ 500 Hz whilst still permitting single-molecule detection and full quantification with negligible photodamage of living bacterial cells.

Results and discussion

Microscopy was performed using a custom-built fluorescence microscope capable of illuminating a biological sample with two independent excitation modes: one for total internal reflection fluorescence (TIRF) and another for slimfield mode. A depiction of the optical path arrangement is shown in Fig. 1, with an actual photograph of the setup during its development in Fig. 2, and an expanded illustration of the slimfield mode at the level of the microscope objective lens is shown in Fig. 3. Using single-molecule TIRF microscopy at video-rate sampling (40 ms per image frame) most of the FPs employed in this study could be identified using custom-written auto-mated image analysis software (see Experimental) as distinct spots of intensity of width 250–300 nm with typical single-molecule intensity traces as reported previously.[14–17] However, constructs containing ECFP, CyPet, pre-activated PS-CFP2

and tagRFP could not be distinguished faithfully above the background detector noise using this method. The CFP-based FPs (ECFP, CyPet and pre-activated PS-CFP2) are known to be relatively dim, each photoactive molecule bleaching on average after emitting $\sim 10^5$ photons, to be compared against the $\sim 10^6$ of EGFP and the 10^7 of EYFP,[6] and to date no study has reported definitive evidence for imaging single molecules of either ECFP or CyPet. Similarly, although tagRFP is not as dim a fluorophore as the CFP family, the absorption peak has its peak at a wavelength of ~ 555 nm and is sub-optimally excited by the 532 nm wavelength laser of our microscope setup. However, using slimfield all FPs in the study could be detected successfully at video-rate sampling. Slimfield illumination simply generates a local excitation field which is greater than that of conventional widefield imaging (such as epifluorescence or TIRF) by a factor of ~ 100 over an area whose diameter is smaller by a factor of ~ 10 (see Experimental). The higher resultant emission intensity from single FPs is greater than the detector noise and thus permits single molecule detection at the expense of a shorter duration of emission before the FP is photobleached. In the case of the tagRFP, the loss in absorption efficiency due to a sub-optimal wavelength of excitation is more than compen-sated for by the increased excitation intensity due to slimfield. Example images from three such FPs are shown in Fig. 4A. Spots of fluorescence intensity have a similar width to those detected in the TIRF mode and photobleach after typically ~ 3–5 image frames (*i.e.* 120–200 ms of illumination), but the intensity of the spots falls off more rapidly with distance from the centre of the illumination field since the Gaussian width of the excitation field profile is only a few microns. Since purely analytical descriptions of Gaussian broadening due to under-filling of an objective lens are known to be prone to artifacts[36] we sampled the intensity profile of the slimfield excitation field
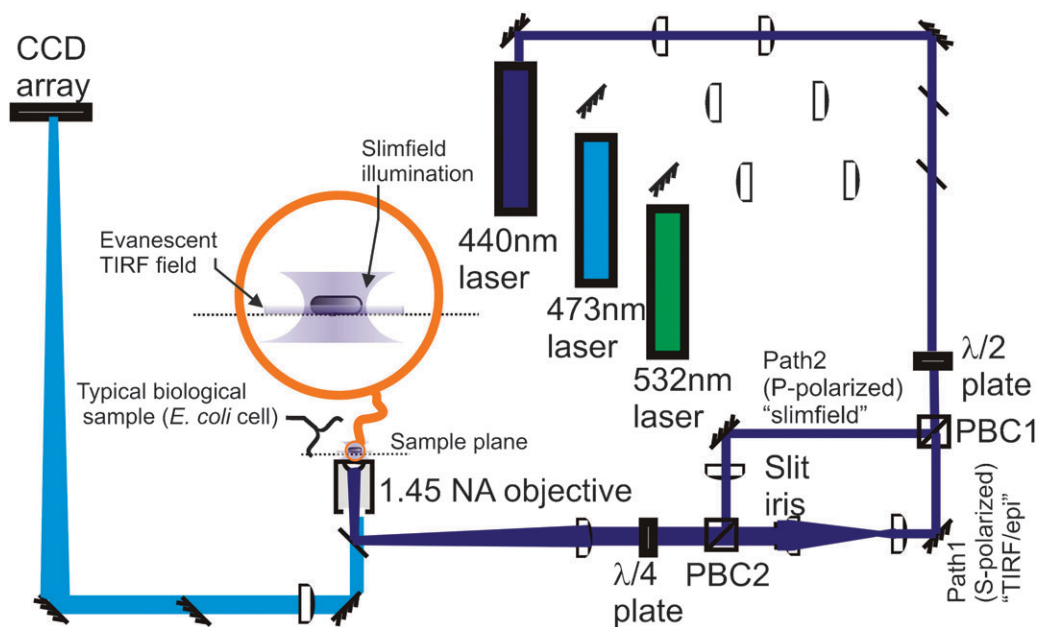

Fig. 1 Schematic of the custom-built multi-colour fluorescence microscope. The optical technology offers user-controllable combinations of TIRF and slimfield excitation modes. A typical biological sample of a single *E. coli* cell is indicated to illustrate the approximate length scale of the two modes.
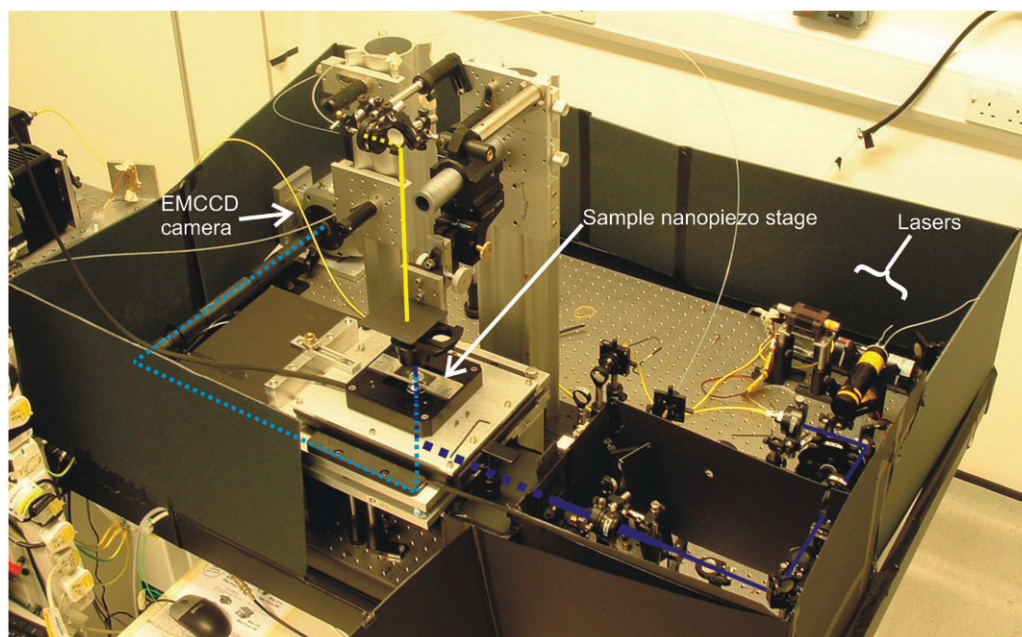
Fig. 2 Photograph of the developing microscope setup. Positions of the excitation lasers, sample stage and camera are indicated. Overlaid lines illustrate positions of an excitation laser beam (dark blue), the emission path (cyan) and the brightfield illumination (yellow).
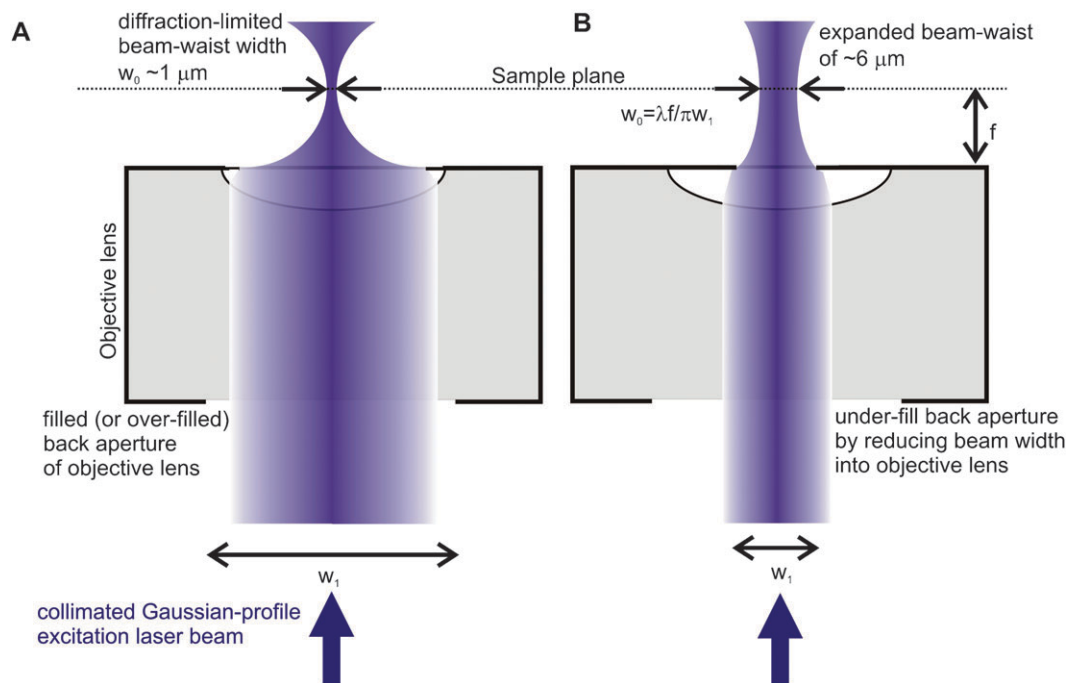

Fig. 3 Schematic depictions of confocal and slimfield excitation modes. The formation of (A) a diffraction-limited excitation volume (for example, as found in conventional confocal microscopy) compared against (B) slimfield illumination for which the back aperture of a high numerical-aperture (NA = 1.45) objective lens is *under*-filled with a collimated laser beam generating a wider field profile at the sample plane compared to (A).

directly using 200 nm fluorescent beads (Molecular Probes) immobilized to the coverslip, and then raster scanned these laterally by movements of the nanopiezo stage across the imaging area, and back again to correct for any photobleaching of the bead. We fitted the corrected bead intensity to a 2D radial Gaussian function $A\exp(-r^2/2\sigma^2)$ where A is the intensity at the centre of the illumination field and r is the distance from the centre, with the optimized field width $\sigma = 3.0 \pm 0.1$ μm. To make quantitative comparisons with the brightness of other molecules across an entire field of view, a small post-processing correction was done to weight the measured pixel intensity at a distance r from the centre of
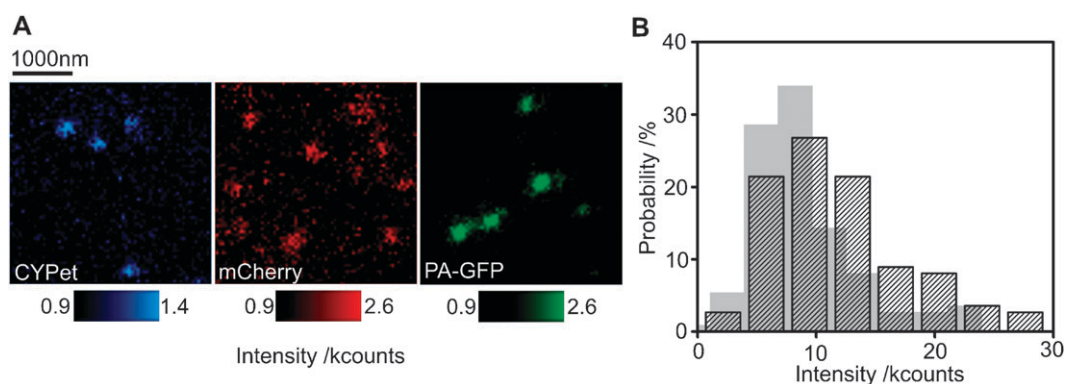
Fig. 4 FP visualization and quantification. (A) Examples of single frame images (40 ms per frame) of single molecules of FPs excited by a 440 nm (CyPet), 532 nm (mCherry) and 473 nm laser (PA-GFP) in slimfield mode. (B) Distribution of total spot intensities (see Experimental) for all detected single molecules of CyPet (grey) with correction for the Gaussian profile of the excitation field (hashed), 112 molecules in total.

the illumination field by a Gaussian correction factor $\exp(r^2/2\sigma^2)$. The effect this correction has on the distribution of fluorescent spot intensities is illustrated in Fig. 4B using the CyPet FP as an example, but for typical *Escherichia coli* bacterial cells (length ~ 2–3 μm) with the cell centre placed at the centre of the slimfield illumination, used later for *in vivo* experiments, this correction factor never exceeded 1.1 (*i.e.* less than a $\sim 10\%$ correction). Table 1 presents the full set of Gaussian-corrected results for all FPs used in the study. This indicates the range of signal-to-noise ratios across the different FPs was 1.0–4.3. To investigate the quantitative effects of reducing the imaging integration time per frame we used the YPet FP as a test model since it had a signal-to-noise ratio in the middle of this range (~ 2.5) for video-rate sampling. We found that single molecules of YPet could still be faithfully detected down to frame integration times as low as 3 ms (Fig. 5). Using an edge-preserving Chung–Kennedy filter[38] allowed measurement of the size of the single-molecule photobleach step (Fig. 5B). Fitting of the pixel intensity intensities within each fluorescent spot (see Experimental) indicated a typical r.m.s. localization precision of ~ 50 nm (Fig. 5C). Extrapolating the signal and noise curves of Fig. 5D indicates an intersection at ~ 0.5 ms. This suggested that sub-millisecond single-molecule imaging above the level of detector noise would be possible using this technique were the camera fast enough.

By modifying the imaging path of the microscope, spectral emissions from the sample could be split on the basis of colour and imaged separately and simultaneously on different halves of the same EMCCD pixel array (Fig. 6A). Here, emissions were divided into a C-channel ($\sim$ cyan light, wavelengths < 560 nm) and a Y-channel ($\sim$ yellow light, wavelengths > 560 nm), with excitation provided from the 440 nm laser. To test the feasibility for high-resolution FRET imaging using the slimfield mode we employed a hybrid FP construct (ECFP-tryp-EYFP) consisting of a single molecule of ECFP linked to a single molecule of EYFP *via* a short amino acid sequence which acted as a proteolytic typsin cleavage site, performing video-rate slimfield excitation. However, since FPs have a continuum emission spectrum over several tens of nm in wavelength, bleed-through into both channels from a single FP is inevitable. Therefore, we first characterized this bleed-through by imaging ECFP and EYFP in separate samples and quantified the fluorescent spot intensities from the C- and Y-channels for each (Fig. 6B,C). This indicated that the proportion α of photon emission flux from an ECFP molecule into the Y-channel was 0.06 ± 0.01 and the proportion β of photon emission flux from an EYFP molecule into the C-channel was 0.07 ± 0.01. Preliminary qualitative observations from imaging the ECFP-tryp-EYFP construct indicated a greater intensity in the Y-channel and a smaller intensity in the C-channel compared to either single FP bleed-through control (Fig. 6D). We then subjected the hybrid construct to proteolysis in the presence of trypsin in an

Table 1 Mean spot intensity values for single FP molecules using video-rate slimfield, error as standard deviation of mean, 25–56 molecules used for each dataset

| Fluorescent protein	Excitation wavelength of laser/nm	Intensity (error)/counts	Signal-to-noise
ECFP	440	8257(1268)	1.1(0.2)
CyPet	440	12 591(699)	1.5(0.1)
Dendra2 (pre-activation)	473	11 695(537)	1.8(0.1)
Dendra2 (activated)	532	13 642(611)	1.9(0.1)
EGFP	473	27 869(7764)	3.3(0.4)
mCherry	532	26 425(2341)	4.3(0.4)
PA-GFP (activated)	473	21 517(2051)	3.1(0.4)
PS-CFP2 (pre-activation)	440	7127(1174)	1.0(0.2)
PS-CFP2 (activated)	473	18 058(1868)	3.3(0.4)
tagRFP	532	8172(780)	1.1(0.2)
EYFP	532	10 994(651)	1.6(0.2)
YPet	532	16 374(1295)	2.5(0.4)
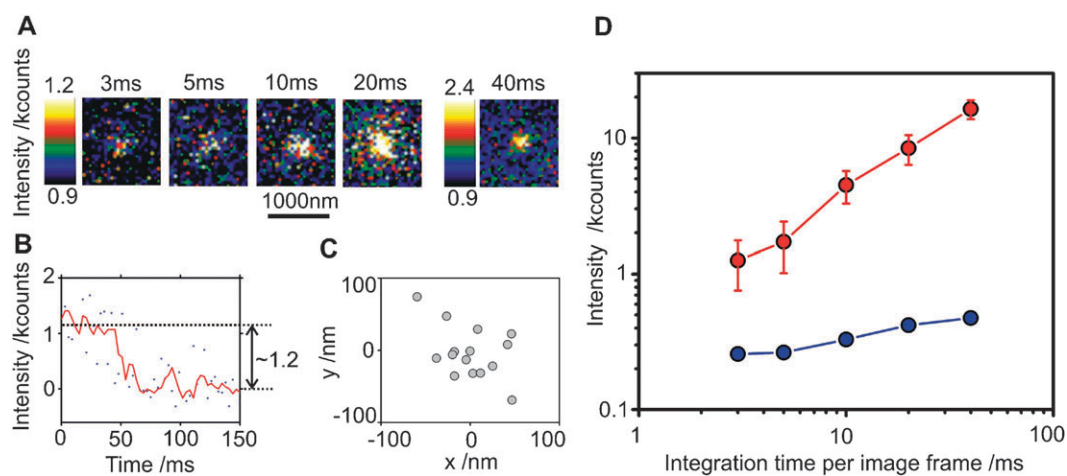
Fig. 5 Pushing down the frame integration time for true 2D imaging of fluorescent proteins. (A) Single false-colour images of different single molecules of YPet taken at frame integration times in the range 3–40 ms. (B) Raw (blue) and filtered (red) spot intensity *versus* time during continuous slimfield illumination of a single YPet molecule at 3 ms per frame, photobleach step-size of ~1.2 kcounts indicated. (C) Scatter-plot indicating the fitted intensity centroid relative to the mean position (see Experimental) for the molecule in (B) during the first 45 ms of illumination over which the molecule is photoactive. This indicates a total r.m.s. value of ~48 nm. (D) Variation of spot intensity for YPet molecules with time per frame (red) compared to equivalent background noise of a region of interest of the same area containing no YPet molecules (blue), standard deviation error bars (for blue trace these are smaller than the plot symbols), between 99 and 443 molecules used in each dataset.
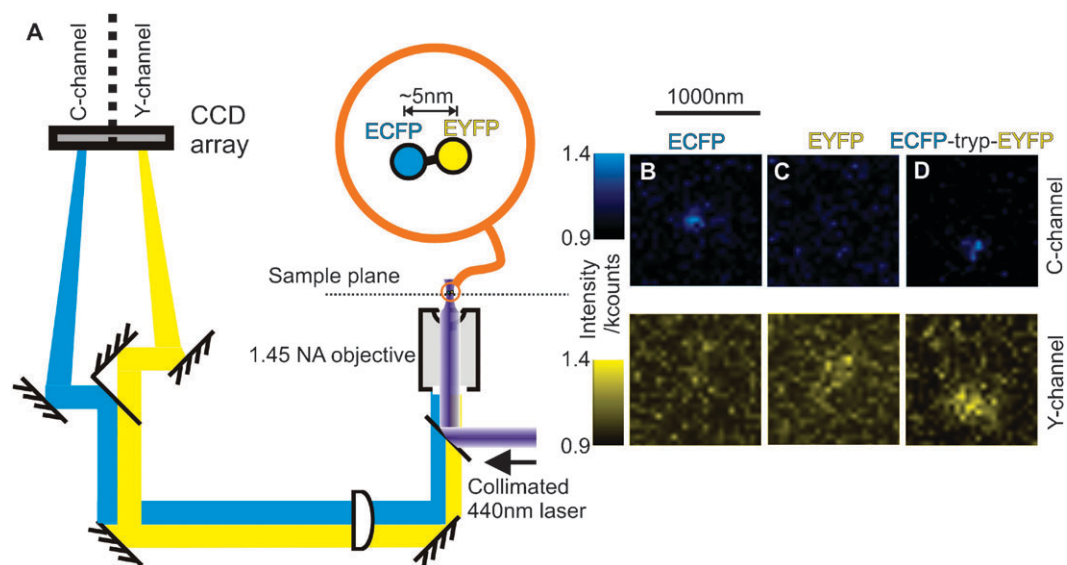

Fig. 6 Dual-view imaging of single FP molecules. (A) Schematic for formation of spectrally separated images on two halves on the same camera CCD array, splitting emissions of less than ~560 nm wavelength into the C-channel, greater than ~560 nm wavelength into Y-channel. Single-molecule images in C- and Y-channels for (B) pure ECFP, (C) pure EYFP and (D) ECFP-tryp-EYFP hybrid construct, all at 40 ms per frame in slimfield mode.

overnight incubation (see Experimental), and imaged the resultant solution. Proteolysis resulted in a increase in the mean C-channel of ~55% with a comparable decrease in the mean Y-channel intensity, indicative of a Förster resonance energy transfer from the donor ECFP component to the acceptor EYFP component in the hybrid construct. Correcting these data from the uncleaved ECFP-tryp-EYFP fusion protein for bleed-through (Table 2) indicated a FRET efficiency of 0.55 ± 0.18.

We performed preliminary live-cell slimfield imaging experiments using two FP fusion *E. coli* bacterial strains.

The first involved a cell strain in which YPet had been genomically fused to one of the DNA polymerase components of the replication fork in the cell cytoplasm. Using slimfield illumination at 3 ms per image frame exciting with the 532 nm laser, distinct spots of fluorescence intensity of width ~300 nm could be seen, generally either one of two spots per cell (Fig. 7A). These complexes are expected to contain either two or three individual polymerase complexes over the extent of a single replication fork of ~15 nm diameter,[39] and thus the same number of YPet molecules should be seen per fluorescent spot. The second cell strain expressed a genomic fusion of the

Table 2 Results from FRET analysis of the CFP-tryp-YFP construct. Error is s.d. of mean value. I_A and I_D are the sensitized acceptor and donor intensities respectively and ε is the FRET efficiency (see Experimental)

Fluorescent protein	C-Channel/counts(error)	Y-Channel/counts(error)	I_A/counts	I_D/counts	ε
ECFP	7510(738)	540(89)	—	—	—
EYFP	265(57)	3980(154)	—	—	—
ECFP-tryp-EYFP proteolysed	7256(2412)	2635(1327)	—	—	—
ECFP-tryp-EYFP intact	4660(1103)	5858(663)	6522(1125)	5333(761)	0.55(0.18)

gfp gene to that of the *flim* which is responsible for expressing a protein known to be involved in the membrane integrated switching complex of the bacterial flagellar motor at a stoichiometry of $\sim$33–35 molecules, but is also delocalized in the cytoplasm as individual molecular subunits.[40] Using slimfield illumination at 2 ms per image frame, which was the hardware limit of our camera when acquiring data from the entire 128×128 pixel array, exciting with the 473 nm laser we could visualise a bright spot of fluorescence intensity of width $\sim$300 nm corresponding to the membrane integrated complex, plus dimmer cytoplasmic subunit components (Fig. 7B). Using the latter strain we also performed a tethered cell assay in which one of the filaments of the flagellar motor was tethered to the glass coverslip resulting in the functional motor forcing the cell body to rotate about that point of attachment.[14] We experimented with photobleaching the GFP components using a range of continuous slimfield exposures between 100–300 ms and measured the cell rotation speed both before and after the bleach using brightfield illumination at 40 ms per frame. Typically cell rotation times were $\sim$1–5 Hz, but we could not detect any significant change to the cell rotation speed due to the slimfield illumination.

Experimental

FP constructs

All cloning steps were performed in *E. coli* XL1-Blue (Stratagene). All oligonucleotides were purchased from Sigma-Aldrich, restriction enzymes and buffers from New England Biolabs. Pfu-polymerase and buffer were obtained from Promega. Plasmids containing the original non-tagged FP genes were pDendra2-B, pPS-CFP2-N (Evrogen),

pLNCyPetMAMM2 and pLNYPetMAMM2 (donated by Peter Daugherty), pECFP-N1 (BDBiosciences), pPAGFP-C1 [A206K] (donated by Jennifer Lippincott-Schwartz[41]) and ptagRFP (Evrogene). Existing plasmids containing His6-tagged FPs were pQE80-YFP, pRSETb_mCherry, and pROD49_mYPet-His. Plasmid pSV46 (donated by Victor Sourjik) contained a His6 tagged construct of ECFP and EYFP, linked by a Trypsin target-site. FP genes were PCR-amplified from the template plasmids, ligated into pQE80 (Qiagen) and confirmed by sequence analysis.

Expression and purification

Single colonies of XL1Blue containing the appropriate FP expression plasmid were grown to an OD_{600} of 0.8 in 2YT-medium. IPTG was added to a final concentration of 100 µM and the culture was incubated at 18 °C for 20 h. Cells were harvested by centrifugation, resuspended in 30 ml of lysis buffer (10% glycerol, 50 mM Tris-HCl, 150 mM NaCl, 10 mM imidazole, 1 mM DTT, pH 8) and stored at −20 °C. Cells were lysed by sonication (Vibracell sonicator, Sonics & Materials Incorporated), the lysate cleared by centrifugation and the proteins purified on a 1 ml Ni-NTA agarose column (Bio-Rad). The concentration of purified proteins was determined by Bradford analysis (Bio-Rad) using BSA as a standard.

Sample preparation

Each FP was separately conjugated to the surface of a standard BK7 glass microscope coverslip using a previously optimized antibody immobilization technique[42] using either rabbit polyclonal IgG anti-GFP antibody (Invitrogen, cat-no. A-11122) for GFP-derived FPs (EGFP, ECFP, EYFP, CyPet, YPet, tagRFP, PA-GFP [A206K]) and Living Colors DsRed
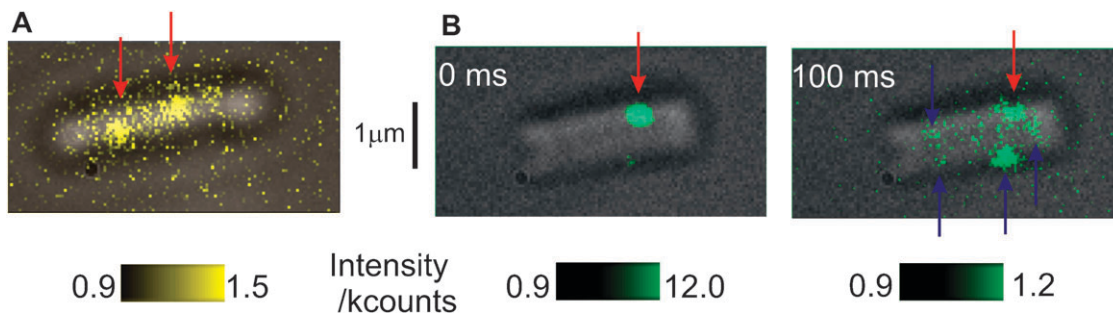

Fig. 7 *In vivo* slimfield imaging of functional *E. coli* bacterial cells. (A) Overlaid brightfield (grey) and slimfield (3 ms single frame, yellow) images for a single *E. coli* cell expressing the *ypet* gene fused to the α component of the DNA polymerase, the positions of detected fluorescent spots (putative replication forks) indicated (red arrows). (B) Overlaid brightfield (grey) and slimfield (2 ms single frame, green) images for a single *E. coli* cell expressing the *gfp* gene fused to *flim* gene which integrates into the bacterial flagellar motor complex. The left panel indicates the first bright frame in the slimfield illumination with the position of the membrane-integrated motor complex indicated (red arrow). The right panel shows an image after 100 ms of slimfield illumination, the original motor complex is shown (red arrow) as are other dimmer spots detected in the cytoplasm (blue arrows).

Polyclonal Antibody (Clontech, cat. no. 632496) for mCherry. For Dendra2 no antibody was used but the protein was found to conjugate to the glass spontaneously with yield lower by a factor of ~3. In brief, a 5 µg ml^{-1} solution of the antibody was prepared in imaging buffer, IB (10 mM potassium phophate, 0.1 mM EDTA, pH 7.4) and injected into a custom-built ~5 µl flow-cell[14] and incubated at room temperature for 5 min. This was then washed with excess IB and then the flow-cell was injected with a 0.1% suspension of 202 nm diameter latex microspheres (Polysciences, Germany) for 2 min to mark the coverslip surface, and washed with excess IB. 10 µl of 15 µg ml^{-1} FP diluted in IB was then injected into the flow-cell, incubated for 10 min at room temperature with unbound protein washed out with excess IB.

Cell strains for *in vivo* imaging

E. coli bacterial cell strains were used which either expressed a genomic construct of the enhanced *gfp* gene to *flim*[49] or a genomic construct of the *ypet* gene to the α gene for the DNA polymerase complex,[50] both kindly donated from work in progress. Each strain expressed the relevant fusion construct at approximately wild-type levels. Cells were grown aerobically with shaking in LB media overnight at 37 °C and sub-cultured aerobically with shaking in M63 minimal glucose media in the morning at 30 °C for 4–6 hours until an OD of ~0.6 was reached. Cells were injected into the microscope flow-cell and either immobilized onto the coverslip surface by a standard protocol using either 0.1% (w/v) poly-L-lysine or tethered *via* a filament using anti-flagellin antibody.[14] Cells were then washed with excess minimal media prior to imaging.

Fluorescence microscopy

The home-built microscope technology incorporated an inverted fluorescence microscope with a x100 Plan Fluor 1.45 NA oil-immersion objective (Nikon UK Ltd, UK) and an *xyz* nanopositioning stage (E-503.00, Physik Instrumente, Germany). Brightfield used a fiber-coupled tungsten–halogen illumination. Laser excitation was available from three separate linearly-polarized DPSS lasers, giving the option for outputting at wavelengths of 440 nm (15 mW, Laser2000 PPMT(LD1650)), 473 nm (50 mW, Laser2000, 473-50-COL-002) or 532 nm (20 mW, Laser2000, PPMT LD1415), expanded ×3. The primary beams were then split into two independently attenuated paths by a polarizing beam-splitting cube generating the separate TIRF and slimfield illumination modes. For the TIRF path the beam was then focussed onto the back-focal-plane of the objective lens *via* a dichroic mirror; for cyan excitation, the 440 nm laser was used in combination with emission filter E515LPv2 with dichroic mirror 505DCLP, for green excitation the 473 nm laser was used with E590LPv2 and 565DCLP and for yellow-red excitation the 532 nm laser was used with E610LPv2 with 560DCLP, a full description of the lasers used for the different FPs is given in Table 1; all filter set components from Chroma.

Controlled lateral movement of this focus position equated to rotation of the emergent angle from the objective lens allowing switching between epifluorescence and TIRF. The field width was ~60 µm, typical intensity ~10 W cm^{-2}.

The separately-shuttered slimfield excitation path directs a collimated laser beam to under-fill the back-aperture of the objective lens. The effect of this is to generate a focussed Gaussian profile at the level of the sample which is expanded laterally to be larger than a diffraction-limited spot. Here we used intensities in the range ~1–7 kW cm^{-2} with a FWHM width of ~7 µm ($\sigma = 3.0 \pm 0.1$ µm) so as to encompass a whole *E. coli* bacterial cell for *in vivo* imaging.

The two separate beams for the TIRF/epifluorescence path and the slimfield path were circularized for polarization by a quarter-wave plate prior to being launched onto the sample.

Fluorescence emissions from the sample were passed through the dichroic mirror, filtered using the relevant band-pass emission filter in the selected filter set and imaged at ~50 nm per pixel in frame-transfer mode at between 25–500 Hz by a 128 × 128 pixel, cooled, back-thinned electron-multiplying charge-coupled-device camera (iXon DV860-BI, Andor Technology, UK). 500 frames with an exposure time in the range 2–40 ms were recorded in each run focussing on the surface of the coverslip for *in vitro* imaging, and at least 10 runs were made for each separate FP or control. For *in vivo* imaging, the focal plane was set at mid-cell height (~0.5 µm) from the coverslip surface. The illuminated field had an area of ~30 µm^2.

Image analysis

Images were analysed using a novel toolkit custom-written in LabVIEW 8.5. Putative fluorescent spots in each image frame were detected automatically using custom-written code to locate circular intensity distributions of width 100–350 nm (Danielsson distance map algorithm). A circular region of interest (ROI) was created around each spot of radius 8 pixels. The intensity in each was approximated as a radial Gaussian plus a uniform baseline of detector background noise. We calculated the intensity contribution due to the FP (the "spot intensity") as follows:

1. We used a circular mask for the contribution of the fluorescent spot of diameter 5 pixels to the ROI centred on the intensity centroid.

2. We convolved intensities within the mask by a 2D radial Gaussian function of fixed width 3 pixels and generated a new estimate for the centroid.[14–17]

3. We iterated steps 1 and 2 either until convergence of the centroid estimate (generally less than 10 loops). For 3 ms per image frame measured for the YPet FP this resulted in an ultimate centroid r.m.s. precision of ~50 nm.

4. We defined the background intensity as the mean intensity within the ROI but outside the circular mask. We defined the spot intensity as the sum of all intensities within the circular mask after subtraction of the background from each individual pixel value.

5. A Gaussian fit was then performed on the spot intensity component optimizing amplitude and width.

This resulted in a fully automatic method for detection of putative fluorescent spots on each separate image frame which could quantify the total pixel intensity minus the background detector noise, the size of the spots and the position of the spot to within typically ~50 nm precision (*i.e.* a super-resolution

estimate ~6 times better than the theoretical diffraction-imposed optical resolution limit). The properties of each spot were compared to those detected in the previous image in a series.[15] Putative fluorescent spots were then confirmed as being "real" if they satisfied the following four criteria:

1. The previous spot position was within 5 pixels of the new position.
2. Spot intensity must change by less than a factor of 2.
3. The width must change by less than a factor of 2.
4. At least 3 consecutive frames satisfy criteria 1–3.

Data were then collated for each FP under each different experimental condition and the distribution of estimated pixel intensity binned on a histogram. Average and s.d. values were estimated for each population.

FRET imaging and analysis

The FRET construct ECFP-tryp-EYFP was excited with the 440 nm laser and imaged with a beam-splitter setup in slimfield mode, where the emitted light was divided into two paths by a dichroic mirror and the cyan light filtered by C-, the yellow by a Y-emission filter, each placed downstream of the filter set itself between the colour-splitting module and the camera. With this method, different emission wavelengths of the same region of the sample could be imaged at the same time. As a control, the same setup was applied to both ECFP and EYFP alone. Putative fluorescent spots in either channel were auto-detected and tracked in consecutive image frames, with a region of interest automatically created at the corresponding position in the other channel. In practice, for the ECFP-tryp-EYFP hybrid construct, most putative spots were detected initially in the C-channel since ECFP is brighter than the EYFP when excited at a wavelength of 440 nm. In a further experiment the ECFP-tryp-EYFP construct was incubated with Trypsin (Sigma Aldrich: TPCD treated from bovine pancreas) overnight at room temperature before imaging. As controls to measure the background signal and possible contaminations, slides with pure PBS and with PBS (containing a maximum of 1% elution buffer) were imaged, indicating no significant fluorescence contamination.

To analyse the FRET data we first denote the following:

I_C = total spot intensity in C-channel.

I_Y = total spot intensity at corresponding position in Y-channel.

I_A = sensitized intensity of ECFP acceptor in FRET pair.

I_D = sensitized intensity of EYFP donor in FRET pair.

α = bleed-through factor of EYFP excited by 440 nm laser into C-channel.

β = bleed-through factor of ECFP excited by 440 nm laser into Y-channel.

Thus, $I_C = I_D + \alpha I_A$ and $I_Y = I_A + \beta I_D$, indicating that $I_A = (\beta I_C + (1 - \alpha)I_Y)/(1 - (\alpha + \beta) + 2\alpha\beta)$,

and $I_D = (\alpha I_Y + (1 - \beta)I_C))/(1 - (\alpha + \beta) + 2\alpha\beta)$.

For the proteolysed FRET construct there was a ~2-fold bias in the detection likelihood for ECFP compared to EYFP due to the greater spot intensity of ECFP compared to EYFP at the excitation wavelength of 440 nm. This resulted in a marginally lower observed mean value in the Y-channel compared to the pure EYFP experiments (Table 2).

We then approximated the FRET efficiency[43] ε by $\varepsilon = I_A/(I_A + I_D)$.

Conclusions

The use of genetically-encoded fluorescent proteins expressed in living cells as single-molecule reporter tags has offered enormous insight into the spatial arrangement of different proteins in functional biological systems. In addition, by monitoring the changes in such spatial patterning as a function of time the dynamics of proteins *in vivo* may be studied. However, limitations in existing technology have to date prevented the dynamics of single fluorescent proteins being studied over a timescale realistic to fast diffusive motion in the cell cytoplasm. Estimates of diffusion coefficients for typical fusion fluorescent protein constructs *in vivo* using non-imaging fluctuation methods such as FCS indicate typical values of the order ~5 μm^2 s^{-1} for cytoplasmic proteins such as those involved in signal-relay processes,[44] typically half that of the untagged wild-type protein.[45] If the imaging integration time per frame is too high for such proteins then their motion will blur out the fluorescence intensity profile making it impossible to detect single protein molecules above the background camera noise. We can estimate the approximate threshold value for this integration time from simple diffusion theory as follows: for three-dimensional diffusion the mean-squared displacement after a time t is given by ~6 Dt where D is the effective diffusion coefficient in that environment; for the fluorescence image to appear reasonably unblurred then the mean distance that the imaged single molecule has diffused in that time needs to be less than its point spread function width, typically ~0.3 μm. This indicates a maximum value for t of ~0.09/(6 × 5) ≈ 3 ms. With our innovation here in microscopy and automated analysis we have demonstrated that single molecules of a commonly used fluorescent protein can be imaged as fast as this. Slimfield generates a relatively compact excitation field compared to conventional widefield imaging techniques such as TIRF and epifluorescence. As a result the intensity of excitation is typically higher by a factor of ~100. The consequent increase in fluorescence emission intensity is then higher than the combined shot, readout and dark noise of the camera detector, which thus permits single-molecule detection in an inexpensive manner requiring relatively simple optical components.

We measured the localization precision for a typical single-molecule FP as ~50 nm when imaging at 3 ms per frame. An earlier study using a technique similar to slimfield by application of a defocussing lens on the side port of a commercial epifluorescence microscope reported single-molecule localization precision of ~20 nm when imaging at 5 ms per frame.[37] However, these previous experiments were performed using photophysically ideal organic dyes which are over an order of magnitude brighter and significantly more photostable than the photophysically poor FPs used here. Correcting for differences in fluorophore brightness and integration time we estimate that the localization precision for our single-molecule FP samples in the earlier imaging setup would have been in excess of ~100 nm. Our new imaging and analysis system has

therefore improved the spatial precision by over a factor of two, which represents a significant advance.

We demonstrate that use of this slimfield mode permits imaging of the relatively dim fluorescent proteins ECFP and CyPet, hitherto unreported. This may be of great potential benefit in a physiological setting for molecular interaction studies since both fluorophores constitute a commonly used donor component for a FRET pairing system when combined with an EYFP or YPet acceptor. By modifying the microscope to separate spectral emissions on the basis of colour onto separate halves of the same camera we were able to quantify the FRET efficiency between ECFP and EYFP in a hybrid fusion protein using single-molecule imaging. The efficiency value of ~ 0.55 is comparable to previous studies utilising a similar ECFP-linker-EYFP arrangement.[46,47] The efficiency corresponds to $R^6/(R_0{}^6 + R^6)$ where R is the separation for the donor and acceptor dipoles and R_0 is the Förster radius for the ECFP/EYFP pair; previous measurements[6] report an R_0 of ~ 4.9 nm, indicating an estimate for R of ~ 5.1 nm. Since the Stokes radius of GFP-like proteins[48] is ~ 2.8 nm this indicates a predominant interaction *within* the equivalent Stokes sphere since the smallest distance between the centres of two such spheres would be ~ 5.6 nm. Presumably therefore the dominant FRET interaction is *via* the cylindrical surfaces of the equivalent barrel structures of ECFP and EYFP. This indicates that our new technology may be capable of monitoring subtle molecular interaction transitions at a single-molecule level *via* commonly employed fluorescent protein FRET pairs.

The preliminary *in vivo* data are still work in progress[49,50] but even so they illustrate that slimfield permits imaging of single low copy-number protein-FP complexes in living cells detectable above the level of background cellular auto-fluorescence. Also, since there is no measurable change to cell rotation speed in tethered cell assays as a result of slimfield illumination this indicates no significant change to the transmembrane proton-motive force (pmf). Since pmf is a very sensitive indicator for cell viability[40] this shows that slimfield illumination used in small doses of a few hundred milliseconds generates no observable photodamage effects, at least in bacteria. The observation of no significant photo-damage may be linked to the fact that although photodamage presumably scales roughly linearly with total number of excitation photons absorbed by the biological sample, the time for a given FP molecule to photobleach scales to a first approximation as the reciprocal of the number of excitation photons absorbed. Thus, if the total maximum exposure time is set to the characteristic photobleach time (for example, a few hundred milliseconds here) then the net photodamage is broadly the same whether illuminating *via* a widefield or slimfield mode. Illuminating beyond the mean photobleach time reveals no useful further fluorescence information barring spurious blinking effects and so is a sensible maximum illumination time to impose.

Modifications we are currently implementing include a strobing system which should allow single $\sim$ millisecond frames to be interleaved with dark periods in which the cell is not exposed to any laser excitation, thereby extending the effective time over which a cell can be observed whilst suffering no significant detrimental effects from either photodamage or photobleaching. In this manner we hope to explore biological processes that occur in the cytoplasm and so require fast millisecond timescale imaging but in which key events within the process may occur over a slower timescale.

Our developments in the hardware of optical technology have been paralleled by progress in new software modules to permit fast, automated, objective detection and quantification of single-molecule images, including precise measurement of size, brightness and localization, the latter to within an accuracy of a few tens of nanometres. The code also permits precise assessment of the mean times taken for single fluorescent protein molecules to photobleach. A secondary future aim besides determining their brightness will be to collate statistics to determine precise changes of photobleaching time under different conditions of both excitation intensity and chemical environment such as pH and chloride ion concentration, all of which are known to be significant factors.[6]

Having now demonstrated the proof-of-principle for this new fast-imaging technology in both controlled *in vitro* and preliminary *in vivo* experiments our next step forward is to apply this system to more complex cellular organisms expressing fluorescent proteins and to explore methods for extending the system into a fully automated high-throughput device.

Acknowledgements

References

1 O. Shimomura, F. H. Johnson and Y. Saiga, *J. Cell. Comput. Physiol.*, 1962, **59**, 223–239.
2 G. M. Hale and M. R. Querry, *Appl. Opt.*, 1973, **12**, 555–563.
3 D. C. Prasher, V. K. Eckenrode, W. W. Ward, F. G. Prendergast and M. J. Cormier, *Gene*, 1992, **111**, 229–233.
4 M. Chalfie, Y. Tu, G. Euskirchen, W. W. Ward and D. C. Prasher, *Science*, 1994, **263**, 802–805.
5 S. Inouye and F. I. Tsuji, *FEBS Lett.*, 1994, **341**, 277–280.
6 R. Y. Tsien, *Annu. Rev. Biochem.*, 1998, **67**, 509–544.
7 D. Chudakov, S. Lukyanov and K. Lukyanov K, *Trends Biotechnol.*, 2005, **23**, 605–613.
8 R. Yuste, *Nat. Methods*, 2005, **2**, 902–904.
9 O. Griesbeck, *Curr. Opin. Neurobiol.*, 2004, **14**, 636–641.
10 I. Ghosh, A. D. Hamilton and L. Regan, *J. Am. Chem. Soc.*, 2000, **122**, 5658–5659.
11 A. Miyawaki, J. Llopis, R. Heim, J. M. McCaffery, J. A. Adams, M. Ikura and R. Y. Tsien, *Nature*, 1997, **388**, 882–887.
12 M. Kneen, J. Farinas, Y. Li and A. S. Verkman, *Biophys. J.*, 1998, **74**, 1591–1599.
13 R. M. Wachter and S. J. Remington, *Curr. Biol.*, 1998, **9**, R628–R629.
14 M. C. Leake, J. H. Chandler, G. H. Wadhams, B. Fan, R. M. Berry and J. P. Armitage, *Nature*, 2006, **443**, 355–358.
15 M. C. Leake, N. P. Greene, R. M. Godun, T. Granjon, G. Buchanan, S. Chen, R. M. Berry and B. C. Berks, *Proc. Natl. Acad. Sci. U. S. A.*, 2008, **105**, 15376–15381.

16 T. Lenn, M. C. Leake and C. W. Mullineaux, *Biochem. Soc. Trans.*, 2008, **36**, 1032–1036.
17 T. Lenn, M. C. Leake and C. W. Mullineaux, *Mol. Microbiol.*, 2008, **70**, 1397–1407.
18 Y. Harada and T. Yanagida, *Cell Motil. Cytoskel.*, 1988, **10**, 71–76.
19 I. Sase, H. Miyata, J. E. T. Corrie, J. S. Craik and K. Kinosita, *Biophys. J.*, 1995, **69**, 323–328.
20 T. Funatsu, Y. Harada, M. Tokunaga, K. Saito and T. Yanagida, *Nature*, 1995, **374**, 555–559.
21 R. M. Dickson, D. J. Norris, Y.-L. Tzeng and W. E. Moerner, *Science*, 1996, **274**, 966–969.
22 A. Ishijima, H. Kojima, T. Funatsu, M. Tokunaga, H. Higuchi, H. Tanaka and T. Yanagida, *Cell*, 1998, **92**, 161–171.
23 D. Axelrod, *J. Cell Biol.*, 1981, **89**, 141–145.
24 D. Axelrod, T. P. Burghardt and N. L. Thompson, *Annu. Rev. Biophys. Bioeng.*, 1984, **13**, 247–268.
25 J. B. Pawley, *Handbook of Biological Confocal Microscopy*, Plenum Press, New York. 1995.
26 M. Minsky, *Scanning*, 1988, **10**, 128–138.
27 M. Göppert-Mayer, *Ann. Phys.*, 1931, **9**, 273–295.
28 W. Kaiser and C. G. B. Garrett, *Phys. Rev. Lett.*, 1961, **7**, 229–231.
29 W. Denk, J. H. Strickler and W. W. Webb, *Science*, 1990, **248**, 73–76.
30 C. J. R. Sheppard and M. Gu, *Optik*, 1990, **86**, 104–106.
31 S. W. Hell, S. Lindek and E. H. Stelzer, *J. Mod. Opt.*, 1994, **41**, 675–681.
32 T. Plakhotnik, D. Walser, M. Pirotta, A. Renn and U. P. Wild, *Science*, 1996, **271**, 1703–1705.
33 B. R. Masters, P. T. C. So and E. Gratton, *Biophys. J.*, 1997, **72**, 2405–2412.
34 C. M. Brown, R. B. Dalal, B. Hebert, M. A. Digman, A. R. Horwitz and E. Gratton, *J. Microsc.*, 2008, **229**, 78–91.
35 E. Gielen, N. Smisdom, M. vandeVen, B. De Clercq, E. Gratton, M. Digman, J.-M. Rigo, J. Hofkens, Y. Engelborghs and M. Ameloot, *Langmuir*, 2009, **25**, 5209–5218.
36 S. T. Hess and W. W. Webb, *Biophys. J.*, 2002, **83**, 2300–2317.
37 T. Schmidt, G. J. Schuetz, W. Baumgartner, H. J. Gruber and H. Schindler, *Proc. Natl. Acad. Sci. U. S. A.*, 1996, **93**, 2926–2929.
38 M. C. Leake, D. Wilson, B. Bullard and R. M. Simmons, *FEBS Lett.*, 2003, **535**, 55–60.
39 A. Johnson and M. O'Donnell, *Annu. Rev. Biochem.*, 2005, **74**, 283–315.
40 H. C. Berg, *Annu. Rev. Biochem.*, 2003, **72**, 19–54.
41 G. H. Patterson and J. Lippincott-Schwartz, *Science*, 2002, **297**, 1873–1877.
42 G. I. Mashanov, D. Tacon, A. E. Knight, M. Peckham and J. E. Molloy, *Methods*, 2003, **29**, 142–152.
43 Y. Arai, A. H. Iwane, T. Wazawa, Y. Yokota, Y. Ishii, T. Kataoka and T. Yanagida, *Biochem. Biophys. Res. Commun.*, 2006, **343**, 809–15.
44 P. Cluzel, M. Surette and S. Leibler, *Science*, 2000, **287**, 1652–1655.
45 J. E. Segall, A. Ishihara and H. C. Berg, *J. Bacteriol.*, 1985, **161**, 51–59.
46 L. He, D. P. Olson, X. Wu, T. S. Karpova, J. G. McNally and P. E. Lipsky, *Cytometry A*, 2003, **55**, 71–85.
47 H. Chen, H. L. Puhl, S. V. Koushik, S. S. Vogel and S. R. Ikeda, *Biophys. J.*, 2006, **91**, L39–41.
48 B. R. Terry, E. K. Matthews and J. Haseloff, *Biochem. Biophys. Res. Comm.*, 1995, **217**, 21–27.
49 N. Delalez, G. Rosser, Q. Xue, I. M. Dobbie, G. H. Wadhams, R. M. Berry, M. C. Leake and J. P. Armitage, unpublished work.
50 R. Reyes-Lamothe, D. J. Sherratt and M. C. Leake, unpublished work.